Atmos. Chem. Phys., 17, 5239–5251, 2017
www.atmos-chem-phys.net/17/5239/2017/
doi:10.5194/acp-17-5239-2017

Atmospheric Chemistry and Physics
Open Access
EGU

Enhanced hydrophobicity and volatility of submicron aerosols under severe emission control conditions in Beijing

Yuying Wang[1], Fang Zhang[1], Zhanqing Li[1,2], Haobo Tan[3], Hanbing Xu[4], Jingye Ren[1], Jian Zhao[5,6], Wei Du[5,6], and Yele Sun[5,6]

[1]State Key Laboratory of Earth Surface Processes and Resource Ecology, College of Global Change and Earth System Science, Beijing Normal University, Beijing 100875, China
[2]Department of Atmospheric and Oceanic Sciences and ESSIC, University of Maryland, College Park, Maryland, USA
[3]Key Laboratory of Regional Numerical Weather Prediction, Institute of Tropical and Marine Meteorology, China Meteorological Administration, Guangzhou 510080, China
[4]Shared Experimental Education Center, Sun Yat-sen University, Guangzhou 510275, China
[5]State Key Laboratory of Atmospheric Boundary Layer Physics and Atmospheric Chemistry, Institute of Atmospheric Physics, Chinese Academy of Sciences, Beijing 100029, China
[6]College of Earth Sciences, University of Chinese Academy of Sciences, Beijing 100049, China

Correspondence to: Zhanqing Li (zli@atmos.umd.edu) and Fang Zhang (fang.zhang@bnu.edu.cn)

Received: 7 December 2016 – Discussion started: 12 January 2017
Revised: 14 March 2017 – Accepted: 18 March 2017 – Published: 24 April 2017

Abstract. A series of strict emission control measures was implemented in Beijing and the surrounding seven provinces to ensure good air quality during the 2015 China Victory Day parade, rendering a unique opportunity to investigate the anthropogenic impact of aerosol properties. Submicron aerosol hygroscopicity and volatility were measured during and after the control period using a hygroscopic and volatile tandem differential mobility analyzer (H/V-TDMA) system. Three periods, namely the control clean period (Clean1), the non-control clean period (Clean2), and the non-control pollution period (Pollution), were selected to study the effect of the emission control measures on aerosol hygroscopicity and volatility. Aerosol particles became more hydrophobic and volatile due to the emission control measures. The hygroscopicity parameter (κ) of 40–200 nm particles decreased by 32.0–8.5 % during the Clean1 period relative to the Clean2 period, while the volatile shrink factor (SF) of 40–300 nm particles decreased by 7.5–10.5 %. The emission controls also changed the diurnal variation patterns of both the probability density function of κ (κ-PDF) and the probability density function of SF (SF-PDF). During Clean1 the κ-PDF showed one nearly hydrophobic (NH) mode for particles in the nucleation mode, which was likely due to the dramatic reduction in industrial emissions of inorganic trace gases. Compared to the Pollution period, particles observed during the Clean1 and Clean2 periods exhibited a more significant nonvolatile (NV) mode throughout the day, suggesting a more externally mixed state particularly for the 150 nm particles. Aerosol hygroscopicities increased as particle sizes increased, with the greatest increases seen during the Pollution period. Accordingly, the aerosol volatility became weaker (i.e., SF increased) as particle sizes increased during the Clean1 and Clean2 periods, but no apparent trend was observed during the Pollution period. Based on a correlation analysis of the number fractions of NH and NV particles, we found that a higher number fraction of hydrophobic and volatile particles during the emission control period.

1 Introduction

China, as the world's second largest economy, is facing severe air pollution problems due to its rapid economic growth. This has led to highly elevated aerosol concentrations, especially in urban regions such as Beijing, Shanghai, and Guangzhou (Hsu et al., 2012; Huang et al., 2014). Every year, high levels of fine particulate matter (PM) have caused many severe haze days in these regions, which may pose a great

health hazard and changes in the regional climate because of aerosol direct and indirect climate effects (Z. Li et al., 2016; G. X. Wu et al., 2016). However, the pollution formation mechanism and the climate effects of aerosols remain highly uncertain due to the highly variable physical and chemical properties of aerosols, as well as complex mechanisms that govern aerosol–climate interactions (Tao et al., 2012; Wang et al., 2014).

Aerosol hygroscopicity and volatility are two important physical properties describing the process of haze formation and its effects on climate. Aerosol hygroscopicity describes the interaction of aerosols and water vapor under sub- and supersaturation conditions and is a vital parameter to the aerosol life cycle, aerosol activation ability, and aerosol direct and indirect climate effects (Swietlicki et al., 2008; Tao et al., 2012; Bian et al., 2014). Aerosol volatility is a physical parameter correlated with carbonaceous aerosols, commonly used to study the aerosol mixing state and aging level (Wehner et al., 2009; S. L. Zhang et al., 2016). To date, there are many ways to measure aerosol hygroscopicity and volatility, but the most popular one is the hygroscopic and volatile tandem differential mobility analyzer (H/V-TDMA) system because it can measure these properties in great detail (Swietlicki et al., 2008).

The Chinese government took many drastic measures to reduce the emissions of air pollutants from industry, road traffic, and construction sites, especially during some great events such as the 2008 Summer Olympic Games and the 2014 Asia-Pacific Economic Cooperation. Swift and drastic improvement in air quality (Huang et al., 2015; Shi et al., 2016) provides unique opportunities to investigate the effects of emissions on air quality. To our knowledge, previous studies have usually focused on aerosol chemistry, sources, and transport (Wang et al., 2010; Gao et al., 2011; Sun et al., 2016b) but not on the effects of emission controls on aerosol hygroscopicity and volatility. Due to the importance of the two factors for describing the process of haze formation as well as the effect on climate, it is necessary to investigate the changes in aerosol hygroscopicity and volatility when emission control measures are in place.

To guarantee good air quality in Beijing during the 2015 China Victory Day parade, the Chinese government implemented much stricter emission control measures than normally done in Beijing and the surrounding seven provinces from 20 August to 3 September. The control measures consisted of a ban on driving vehicles every other day, shutting down or limiting factory production, stopping construction activities, and so on. These emission control measures successfully ensured a continuous stretch of 15 days of blue sky, vividly named "Parade Blue" (H. Li et al., 2016). During and after the parade emission control period, we conducted in situ measurements of submicron aerosol chemical and physical properties in Beijing. Size-resolved chemical compositions were also obtained (Zhao et al., 2017). The average concentration of PM less than 1 µm in diameter (PM_1) was

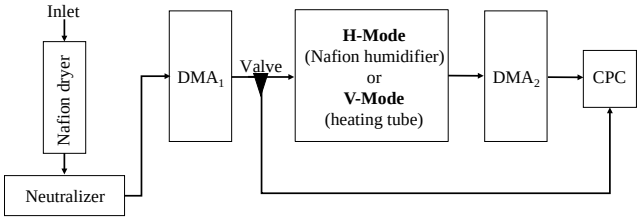

Figure 1. A schematic diagram of the hygroscopic and volatile tandem differential mobility analyzer (H/V-TDMA).

19.3 µg m^{-3} during the parade emission control period, 57 % lower than that after the control period. All chemical species decreased during the control period, but their decreasing percentages were different.

This study period is unique for investigating aerosol properties during periods of low PM levels. This paper will further evaluate the impact of emission controls on the hygroscopicity and volatility of submicron aerosols, which may bring some insight into how to reduce pollution in the future. Furthermore, investigating aerosol hygroscopicity and volatility with and without emission controls will help in understanding environmental and climate changes in general. This paper is structured as follows. Section 2 describes the instrumentation and data used, and Sect. 3 introduces the methods to data analysis. Aerosol hygroscopicity and volatility during different periods were compared and discussed in Sect. 4. Conclusions and summary are given in Sect. 5.

2 Experimental methods

2.1 Sampling site and meteorology

The submicron aerosol hygroscopicity and volatility were measured in situ from 26 August to 7 October 2015 using the H/V-TDMA system located at the Institute of Atmospheric Physics (IAP), Chinese Academy of Sciences (39.97° N, 116.37° E), which is located between the north third and fourth ring roads in northern Beijing. The sampling instruments were put into a white container at ground level and an air conditioner was used to maintain the temperature at 20–25 °C inside the container. Meteorological variables, including temperature (T), relative humidity (RH), wind speed (WS), and wind direction (WD), were measured at different heights of a 325 m meteorological tower, the tower located ∼ 20 m west of the container. To eliminate the influence of buildings on wind, we selected the 280 m WD and 8 m WS as references in this study. Simultaneously, particle number concentrations (10–600 nm) were also measured by a scanning mobility particle sizer (SMPS) located at the 260 m level of the tower. The SMPS is equipped with a long differential mobility analyzer (DMA; model 3081A, TSI Inc.) and a condensation particle counter (CPC; model 3775, TSI Inc.). In addition, aerosol chemical composition was measured using

a high-resolution aerosol mass spectrometer (HR-AMS) and an aerosol chemical speciation monitor (ACSM), deployed at ground level and at the 260 m level of the tower respectively. The HR-AMS was situated in a sampling room located on the rooftop of a two-story building ($\sim$ 8 m), $\sim$ 25 m north from the container. An analysis of the aerosol chemical composition has been done (Zhao et al., 2017).

2.2 Instrumentation and operation

The H/V-TDMA system developed by the Guangzhou Institute of Tropical and Marine Meteorology (ITMM) was used to measure the submicron aerosol hygroscopicity and volatility. The H-TDMA system (H-mode) shown in Fig. 1 consists of four main parts: (1) a Nafion dryer (model PD-70T-24ss, Perma Pure Inc., USA) and a bipolar neutralizer (Kr85, TSI Inc.). The Nafion dryer ensured that the RH of the sample flow was below 20 % over the entire measurement period, and the bipolar neutralizer was used to equilibrate the charge of particles (Wiedensohler, 1988). (2) The first differential mobility analyzer (DMA_1; model 3081L, TSI Inc.) was used to select quasi-monodisperse particles of a certain diameter through a fixed electric voltage. The diameters selected were 40, 80, 110, 150, and 200 nm. (3) A Nafion humidifier (model PD-70T-24ss, Perma Pure Inc., USA) was used to humidify the aerosol flow from the DMA_1 to a defined RH. In the study, we set RH to 90 %. (4) The second DMA (DMA_2, same model as the DMA_1) and a CPC (model 3772, TSI Inc.) were used together to measure the number size distribution of the humidified particles. An automated valve located between the DMA_1 and the Nafion humidifier directly connects the DMA_1 with the CPC. This can be used to measure the 10–400 nm particle number size distribution (PNSD) by varying the electric voltage of the DMA_1. Details about the design of the H-TDMA system and its applications are given by Tan et al. (2013a).

The design of the V-TDMA system (V-mode) is similar to that of the H-TDMA system, except that the Nafion humidifier in the V-TDMA system was replaced by a heating tube that induces the evaporation of volatile materials. The heating tube was an 80 cm long stainless steel tube with an inner diameter of 8 mm. With a sample flow rate of 1.0 L min^{-1}, its residence time ($\sim$ 2.4 s) in the heated section is sufficient for the volatile materials to be effectively vaporized (Cheung et al., 2016). In this study, the heating temperature was set to 300 °C. The residual particles of volatile compounds at this temperature, such as sulfates, nitrates, and most organics, are mainly refractory nonvolatile organic carbon (such as polymer-type organics) and sea salts (Philippin et al., 2004; Wehner et al., 2009; Cheung et al., 2016; Ma et al., 2016). Particle were measured at the diameters of 40, 80, 110, 150, 200, and 300 nm. The H/V-TDMA system has been successfully used in previous studies (Tan et al., 2013b, 2016; Cheung et al., 2016).

The hygroscopic growth factor (GF) at a given RH and the volatile shrink factor (SF) at a certain temperature are defined as the ratio of the conditional diameter to the dry diameter with respect to RH and T:

$$\mathrm{GF} = D_\mathrm{p}(\mathrm{RH}) \,/\, D_\mathrm{0dry}, \quad (1)$$

$$\mathrm{SF} = D_\mathrm{p}(T) \,/\, D_\mathrm{0dry}. \quad (2)$$

Here, D_p (RH) refers to the particle diameter measured at RH = 90 %, D_p (T) refers to the particle diameter measured at T = 300 °C, and D_0dry refers to the dry diameter set by the DMA_1. The measured distribution function (MDF) versus GF or SF can be calculated with the number concentration from CPC data downstream from the DMA_1 and the DMA_2. However, the MDF is a skewed and smoothed integral transformation of the particles' actual growth/shrink factor probability density function (GF-PDF or SF-PDF) due to the effect of the DMA diffusion transfer function (Swietlicki et al., 2008; Gysel et al., 2009). In this study, the TDMAfit algorithm (Stolzenburg et al., 1988, 2008) was used to retrieve the GF-PDF and the SF-PDF. The TDMAfit algorithm assumes that groups in the PDF following one or more lognormal distribution functions (Gaussian shape), thus allowing for the possibility that particles of a given type are not all identical.

3 Data analysis

3.1 Hygroscopicity parameter

According to the Köhler theory (Petters et al., 2007), the hygroscopicity parameter κ can be used to depict the hygroscopicity of particles at different RHs. Using H-TDMA data, κ is calculated as

$$\kappa\,(\mathrm{GF}, D_\mathrm{d}) = (\mathrm{GF}^3 - 1)\cdot\left[\frac{1}{\mathrm{RH}}\exp\left(\frac{4\sigma_\mathrm{s/a}M_\mathrm{w}}{\mathrm{RT}\rho_\mathrm{w}\mathrm{D_d GF}}\right) - 1\right], \quad (3)$$

where RH is the default value of the H-TDMA, $\sigma_\mathrm{s/a}$ is the surface tension of the solution/air interface, M_w is the molecular weight of water, R is the universal gas constant, T is the temperature, ρ_w is the density of water, $\mathrm{D_d}$ is the diameter of the dry particles (equivalent to D_0dry as mentioned above), and GF is from Eq. (1). In this study, T used in the κ calculation is 23 °C (the average temperature of the inner container) and $\sigma_\mathrm{s/a}$ is assumed to be the same as the surface tension of the pure water–air interface (about 0.0723 N m^{-1} at 23 °C).

3.2 Statistics of κ-PDF and SF-PDF

The probability distribution function of κ (κ-PDF, $c(\kappa, D_\mathrm{d})$) derived from the GF-PDF was normalized as $\int c(\kappa, \mathrm{D_d})d\kappa = 1$. The ensemble mean hygroscopicity parameter is then defined as the number-weighted mean GF of κ-PDF over the whole κ range:

$$\kappa_\mathrm{mean} = \int_0^\infty \kappa c(\kappa, \mathrm{D_d})\mathrm{d}\kappa. \quad (4)$$

The standard deviation of κ-PDF is

$$\sigma_{\kappa-\mathrm{PDF}} = \left(\int_0^\infty (\kappa - \kappa_{\mathrm{mean}})^2 c(\kappa, \mathrm{D_d}) \mathrm{d}\kappa \right)^{\frac{1}{2}}. \quad (5)$$

The calculated statistical parameters of SF-PDF (c(SF, $\mathrm{D_d}$)) are similar to those of κ-PDF, so SF can be used instead of κ and c(SF, $\mathrm{D_d}$) instead of $c(\kappa, \mathrm{D_d})$ in these equations.

3.3 Classification of different hygroscopic and volatile groups

The mixing state of ambient aerosol particles is complex due to different sources, different aging processes, and so on. Different hygroscopic and volatile groups had been used around the Beijing region using H-TDMAs and V-TDMAs (Massling et al., 2009; Liu et al., 2011; S. L. Zhang et al., 2016). Based on previous studies and our measurements (Fig. S1 in the Supplement), ambient aerosol particles were classified into three hygroscopic groups and three volatile groups, where κ and SF are used here to define the boundaries for each group:

- nearly hydrophobic (NH): $\kappa < 0.1$;
- less hygroscopic (LH): $0.1 \leq \kappa < 0.2$;
- more hygroscopic (MH): $0.2 \leq \kappa$;
- nonvolatile (NV): SF ≥ 0.88;
- slightly volatile (SV): $0.88 >$ SF ≥ 0.55;
- very volatile (VV): SF < 0.55.

The number fraction (NF) for each hygroscopic group with the boundary of $[a, b]$ is defined as

$$\mathrm{NF} = \int_a^b c(\kappa, Dp) \mathrm{d}\kappa. \quad (6)$$

The number fraction of each volatile group also can be calculated using a similar equation.

4 Results and discussion

4.1 Overview of measurements

4.1.1 Meteorological conditions during the sampling period

Air quality has a strong correlation with local WD in Beijing. Previous studies have shown that high PM concentrations usually correspond to southerly winds, while low PM concentration are generally related to northerly winds, because there were more high-concentration air pollutants from source locations south of the Beijing area (Wehner et al., 2008; Wang et al., 2010; Gao et al., 2011). Figure 2 displays time series of WD at 280 m, WS at 8 m, ambient T, and RH. During the emission control period, the prevailing winds were northerly, except for the period from 29 to 30 August due to the influence of accumulated precipitation. During the non-control period, the prevailing winds changed due to the influence of weather systems. Two cold fronts passed on 2 different days: on the night of 9 September and in the early morning of 30 September. During these frontal passages, the prevailing winds were northerly, but on other days the prevailing winds were southerly and the meteorological parameters showed obvious diurnal cycle patterns. Over the measurement period, the average ambient T and RH were 21.9 °C and 62.4 % respectively.

4.1.2 Time series of κ-PDF and SF-PDF, and the division of clean and pollution periods

Figure 3 shows the time series of 10–400 nm particle mass concentrations ($\mathrm{PM_{10-400\,nm}}$) derived from PNSD measurements and the time series of κ-PDF and SF-PDF with 40 and 150 nm particles as examples. Particles with D_p equal to 40 nm represent local-impacted particles and particles with D_p equal to 150 nm represent regional-transport particles. Several haze events during the non-control period can be seen from the time series of $\mathrm{PM_{10-400\,nm}}$, which shows the rapid accumulation of particle mass concentration. Based on mass concentrations and weather conditions, we selected several clean and pollution periods to study the differences in aerosol hygroscopicity and volatility for two different cases (Fig. 3). To further study the effect of emission controls, we divided the clean period into two periods: Clean1 (control clean period) and Clean2 (non-control clean period). During the Clean1, Clean2, and Pollution periods, the average $\mathrm{PM_{10-400\,nm}}$ was 6.9 ± 2.8, 6.0 ± 4.2, and $51.0 \pm 25.6\,\mu\mathrm{g\,m^{-3}}$ respectively. There was no significant precipitation during the three selected periods. The time series of κ-PDF and SF-PDF (Fig. 3b–e) showed evident changes and fluctuations in the measurements. The prominent differences in κ-PDF and SF-PDF during the three periods will be discussed in the following sections.

A wind rose diagram (Fig. S2) was used to compare winds during the different periods. During the Clean1 and Clean2 periods, wind directions were similar, mainly from the north and northwest. During the Pollution period, the wind direction had the characteristics of mountain–valley breezes where the wind direction changed routinely at midnight and changed the wind direction from southerly to northerly (Fig. 2). The change in wind direction at night would reduce pollution in the short term (Sun et al., 2016b). Even so, the prevailing wind direction was southerly during the Pollution period (Fig. S2), which was favorable for the transport of pollutants from the more populated and more industrialized south and southeast to Beijing. The mean WS and RH were

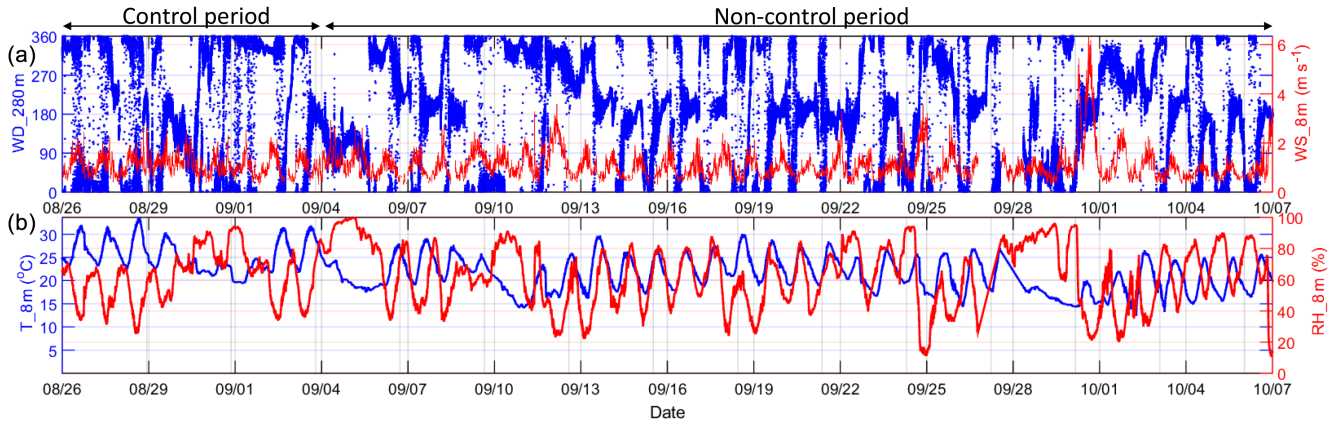

Figure 2. Time series of **(a)** wind direction at 280 m (in blue) and wind speed at 8 m (in red) and **(b)** ambient temperature at 8 m (in blue) and relative humidity at 8 m (in red) during the control and non-control periods at the Beijing site (26 August–6 October 2015).

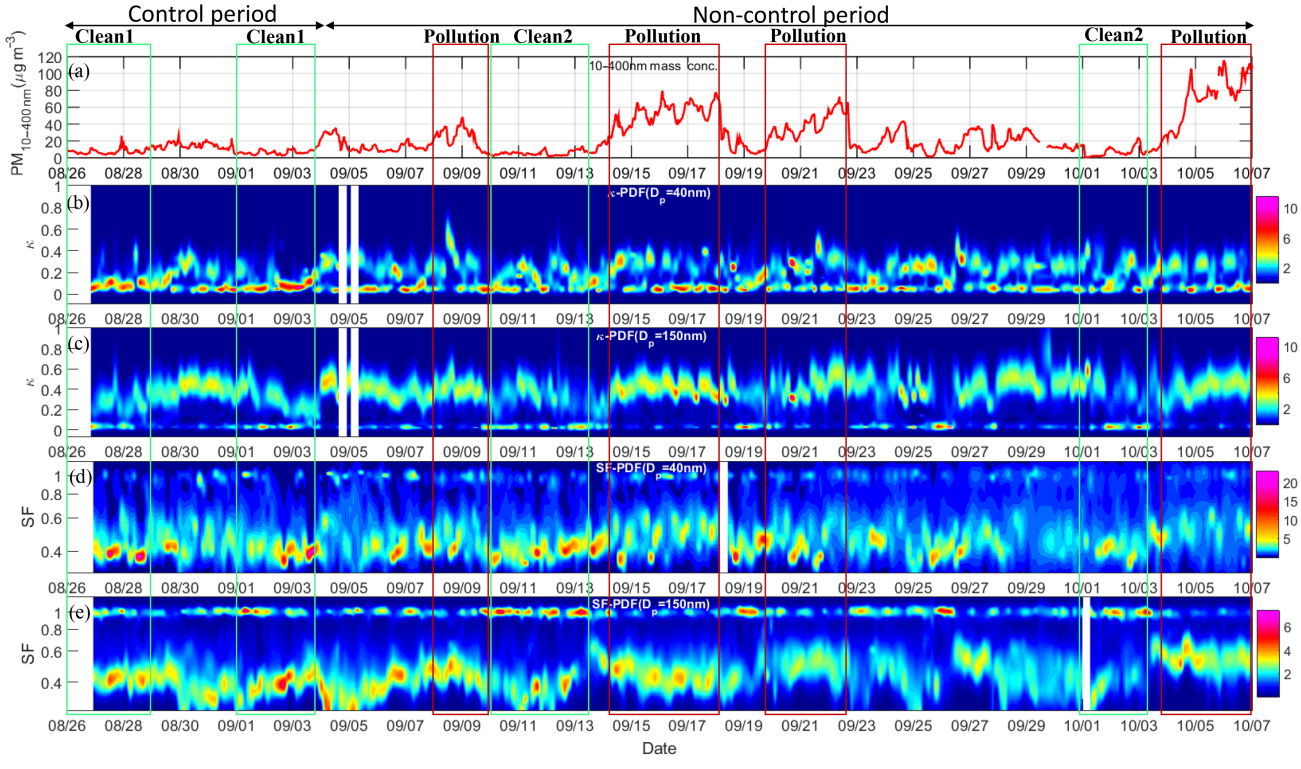

Figure 3. Time series of **(a)** 10–400 nm aerosol mass concentration ($PM_{10-400\,nm}$; assuming that the aerosol density is $1.6\,g\,cm^{-3}$), hygroscopicity parameter κ distributions (κ-PDF) for **(b)** 40 nm and **(c)** 150 nm particles at RH = 90 %, and volatile shrink factor distributions (SF-PDF) for **(d)** 40 nm and **(e)** 150 nm particles at $T = 300\,°C$.

similar during all periods, but the mean temperature during the Clean2 period was lower than during the other periods due to the influence of cold fronts (Table S1 in the Supplement). In summary, the meteorological parameters of the Clean1 and Clean2 cases were similar expect for the ambient T. This provided the opportunity to compare the differences in aerosol properties between control and non-control periods. The high level of PM during the Pollution case can also provide a good opportunity to compare differences between clean and polluted environments.

4.2 Diurnal variation

4.2.1 Diurnal variation in the aerosol size distribution

Figure 4a shows the diurnal variation in total number concentration of 10–400 nm particles ($N_{10-400\,nm}$). In general,

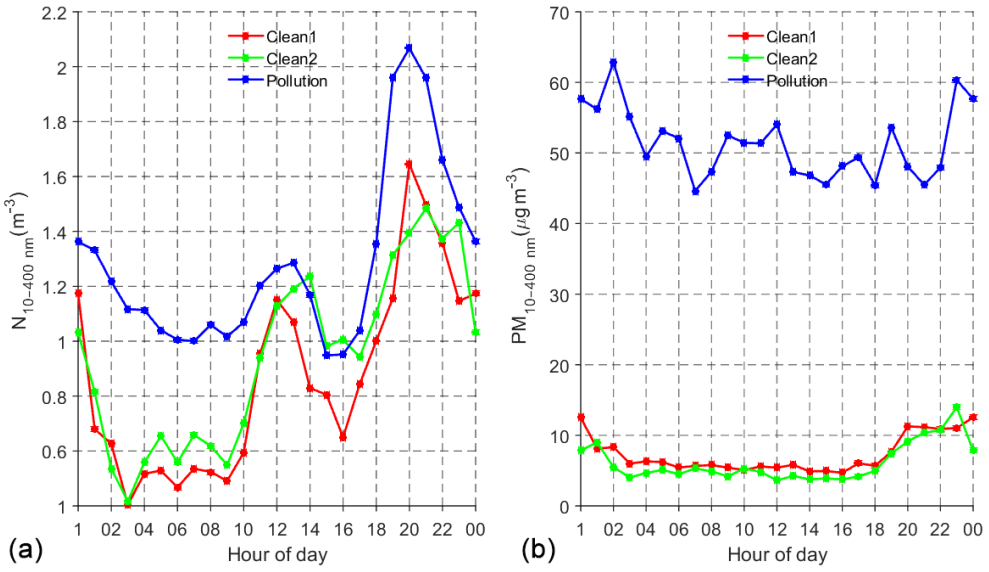

Figure 4. Diurnal variation in mobility diameter (D_p) 10–400 nm particles **(a)** number concentration ($N_{10-400\,nm}$) and **(b)** mass concentration ($PM_{10-400\,nm}$) for the Clean1 (in red), Clean2 (in green), and Pollution (in blue) cases.

$N_{10-400\,nm}$ is higher at night and lower during the day due to the influence of changes in the planetary boundary layer (PBL). However, a significant peak in $N_{10-400\,nm}$ is also seen at noontime because of new particle formation (NPF) events (Fig. S3). NPF started at about 0900 local time (LT) during the Clean1 and Clean2 periods. During the Clean1 period, the $N_{10-400\,nm}$ peak was lower than that observed during the Clean2 period, and the peak in the Clean1 case appeared 2 h earlier than that in the Clean2 case (12:00 LT during Clean1 and 14:00 LT during Clean2). This illustrates that the strength of the NPF was weaker during the Clean1 period than during the Clean2 period and that it was likely related to the decrease in precursors during the Clean1 period. H. Li et al. (2016) have reported that during the parade control period, the precursors SO_2, NO_x, and volatile organic compounds (VOCs) decreased by 36.5, 49.9, and 32.4 % respectively. The relatively higher ambient temperature during the Clean1 period was also unfavorable for NPF (Kulmala et al., 2004).

Figure 4b compares diurnal variations in total mass concentration of 10–400 nm particles ($PM_{10-400\,nm}$) during the three periods. No clear increase in $PM_{10-400\,nm}$ is seen while $N_{10-400\,nm}$ sharply increases during the Clean1 and Clean2 daytime periods. This is because the D_p for most particles was less than 100 nm, which contributed little to $PM_{10-400\,nm}$. During the Clean1 and Clean2 periods, $PM_{10-400\,nm}$ had an obvious diurnal variation, which could be attributed to the evolution of the PBL. As is known, the lower PBL at night aids in the accumulation of pollutants (Achtert et al., 2009). However, this effect was weak in the pollution case because of the change in wind direction from southerly to northerly at midnight, which could partly offset the influence of the PBL.

4.2.2 Diurnal variation in aerosol hygroscopicity

Figure 5a shows the diurnal variation in size-resolved κ_{mean} during the three periods. κ_{mean} shows a peak during daytime and is always higher than that observed during nighttime. This is because more highly aged particles due to photochemical reactions cause the increase in κ_{mean} during daytime. In the evening, thermal inversion would cap the ground level and a number of low-hygroscopic primary particles (like black carbon, BC) emitted from local diesel trucks and heavy-duty vehicles results in the decrease in κ_{mean} during nighttime (Liu et al., 2011; S. L. Zhang et al., 2016). During the Clean2 period, there is another obvious peak at about 03:00 LT in the early morning, likely related to the increase in nitrate. Because there was a large amount of NO_x emitted from traffic sources in the evening during the non-control period, with the PBL height reduction and ambient temperature decrease, NO_x could be transformed into hydrophilic nitrate rapidly through NO_3 and N_2O_5 (Dall'Osto et al., 2009). This was also verified from comparisons of the nitrate diurnal cycle with and without emission controls (Zhao et al., 2017).

Figure 5b shows the diurnal variation in κ-PDF for particles with D_p equal to 40 nm (i.e., local-impacted particles) during the three periods. During the Clean1 period, the κ-PDF has a quasi-unimodal shape (only in the hydrophobic mode). During NPF events, κ_{mean} increases slightly, indicating that 40 nm particles from local sources were always hydrophobic and a very small number of hygroscopic particles were produced through the nucleation and growth from gaseous precursors. This is likely because the secondary formation of hydrophilic sulfate and nitrate was suppressed due to low concentrations of SO_2 and NO_x during the parade con-

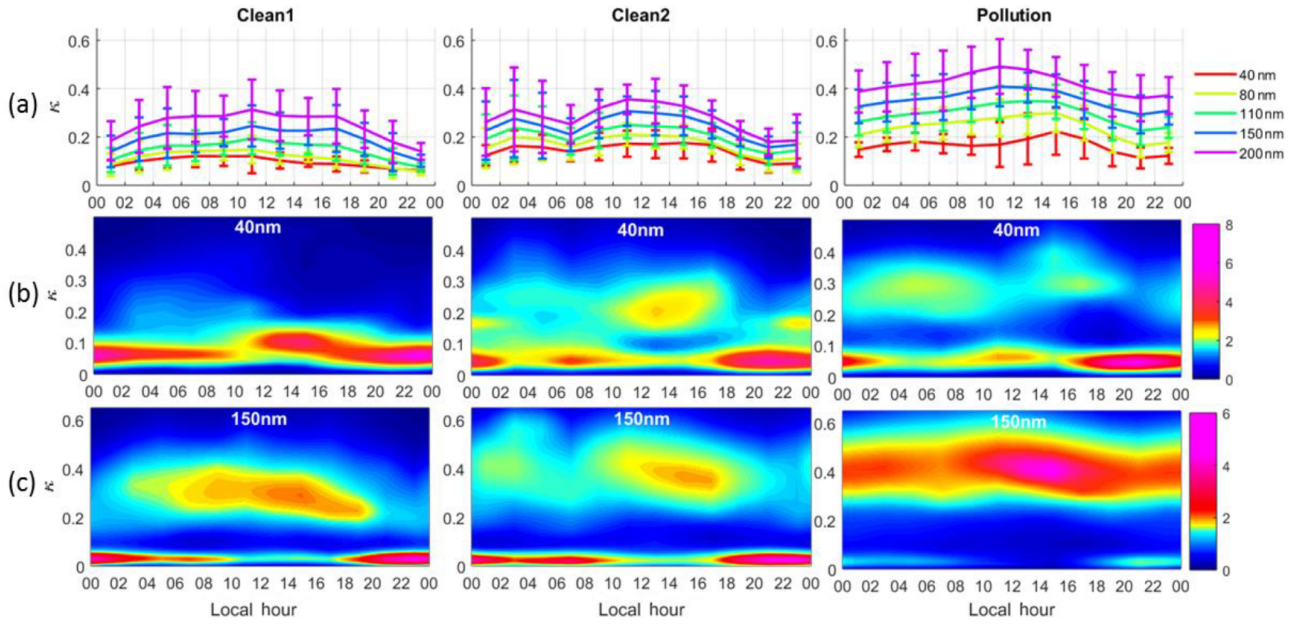

Figure 5. Diurnal variations in **(a)** mean κ (κ_{mean}) for different mobility diameters, **(b)** κ-PDF for particles with D_p equal to 40 nm, and **(c)** κ-PDF for particles with D_p equal to 150 nm during the Clean1, Clean2, and Pollution periods.

trol period (H. Li et al., 2016). Most of the new particles should consist of less-hygroscopic organics that are formed by oxidation and condensation of VOCs. By contrast, during the Clean2 period, the κ-PDF with D_p of 40 nm shows either a bimodal or quasi-trimodal distribution and exhibits a large diurnal variation during the day. Interestingly, when the NPF event occurred at about 09:00 LT, the number fraction of the hydrophobic mode quickly decreased and the hydrophilic mode increased (Fig. 5b), suggesting the conversion of externally mixed particles to internally mixed particles due to the species condensation (sulfate, nitrate, and organics) from the photochemical reaction of SO_2, NO_x and VOCs. A similar phenomenon was also observed by Z. J. Wu et al. (2016). For the Clean1 case, much less of these gases was in the atmosphere due to the emission control. Around 17:00 LT, the fraction of hydrophobic-mode particles increased again, mainly due to substantial traffic emissions at rush hour. However, during the Pollution period, the κ-PDF shows a bimodal shape during the day. The hydrophilic mode becomes stronger in the early morning and in the afternoon, which is attributed to the NO_x heterogeneous reactions at night and the aging and growth of pre-existing particles during the day.

In summary, the diurnal variations in κ-PDF for 40 nm particles were significantly different during the three periods and the emission control appeared to change the diurnal pattern of κ-PDF, mainly due to the decrease in gas precursors, like SO_2 and NO_x, the reduction of which will suppress the formation of hydrophilic matter.

However, the κ-PDF for 150 nm D_p particles (i.e., regional-transport particles) had a similar diurnal variation pattern during the three periods (Fig. 5c) and showed NH and MH modes. The number fraction of the MH mode increased significantly during daytime. There are different reasons for the diurnal variations. One reason is that during daytime, strong photochemistry can produce a large number of condensable vapors, such as sulfuric acid and secondary organic species, which can condense onto pre-existing particles and enhance their water-absorbing capacity (Z. J. Wu et al., 2016). Another reason is that when the sun rises, the PBL height increases and older particles are well-mixed, making them more hydrophilic (S. L. Zhang et al., 2016). However, the MH mode is much more evident for the Pollution case and may be related to the higher mass fractions of inorganic salts and more internally mixed particles during the Pollution period.

4.2.3 Diurnal variation in aerosol volatility

Figure 6a shows the diurnal variation in SF_{mean}, which shows similar trends for all three cases, with the lowest SF_{mean} in the afternoon (12:00–15:00 LT) and the highest SF_{mean} in the morning (07:00–09:00 LT) for all particles with D_p ranging from 40 to 300 nm. The diurnal variations illustrate that particles had a higher volatility during the day than at night. This feature is more obvious for those small particles observed during the Clean1 period. During the Clean1 period, particle volatility increased dramatically (i.e., SF_{mean} decreased) along with the occurrence of NPF events, suggesting that the earliest newly formed matter (before $\sim$ 12:00 LT) was always volatile at 300 °C. As stated previously, during the Clean1 period VOC has a weaker decrease than SO_2 and NO_x; this would lead to more VOC-formed organic parti-

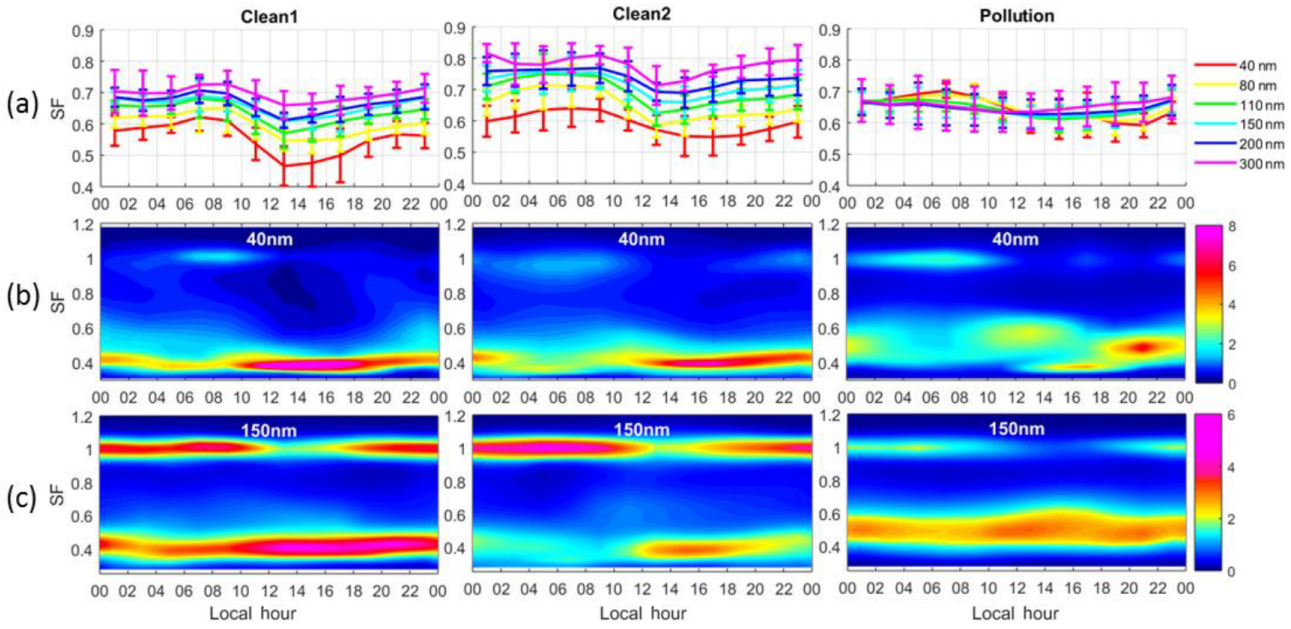

Figure 6. Diurnal variation of **(a)** mean SF (SF_{mean}) for different mobility diameters, **(b)** SF-PDF for particles with D_p equal to 40 nm, and **(c)** SF-PDF for particles with D_p equal to 150 nm during the Clean1, Clean2, and Pollution periods.

Table 1. Summary of size-resolved mean κ, the κ-PDF growth spread factor ($\sigma_{\kappa-PDF}$), size-resolved mean SF during the selected three periods, and the change in percentage of κ and SF during the control Clean1 period compared with the non-control Clean2 period.

		40 nm	80 nm	110 nm	150 nm	200 nm	300 nm
Clean1	κ	0.10 ± 0.05	0.11 ± 0.06	0.15 ± 0.07	0.20 ± 0.10	0.25 ± 0.12	–
	$\sigma_{\kappa-PDF}$	0.08 ± 0.03	0.10 ± 0.03	0.12 ± 0.03	0.14 ± 0.03	0.15 ± 0.04	–
	SF	0.55 ± 0.08	0.60 ± 0.07	0.64 ± 0.06	0.66 ± 0.05	0.67 ± 0.05	0.70 ± 0.06
Clean2	κ	0.14 ± 0.06	0.17 ± 0.08	0.20 ± 0.10	0.24 ± 0.12	0.28 ± 0.13	–
	$\sigma_{\kappa-PDF}$	0.11 ± 0.04	0.13 ± 0.03	0.15 ± 0.03	0.17 ± 0.03	0.19 ± 0.04	–
	SF	0.60 ± 0.06	0.66 ± 0.07	0.70 ± 0.07	0.72 ± 0.07	0.74 ± 0.06	0.78 ± 0.06
Pollution	κ	0.16 ± 0.08	0.24 ± 0.08	0.30 ± 0.09	0.36 ± 0.10	0.42 ± 0.12	–
	$\sigma_{\kappa-PDF}$	0.12 ± 0.02	0.13 ± 0.02	0.14 ± 0.02	0.14 ± 0.02	0.15 ± 0.04	–
	SF	0.65 ± 0.06	0.65 ± 0.06	0.65 ± 0.05	0.65 ± 0.05	0.65 ± 0.06	0.66 ± 0.07
$\frac{(Clean1-Clean2)}{Clean2}$	κ	−32.0 %	−31.9 %	−26.1 %	−17.5 %	−8.5 %	–
	SF	−7.5 %	−9.4 %	−9.2 %	−8.7 %	−10.1 %	−10.5 %

cles formed, which are normally highly volatile. Therefore, the highest volatility was observed during the Clean1 period. Wehner et al. (2009) also showed that ∼ 97 % of newly formed particles are volatile because they are dominated by sulfate and organics. With the processes of particle aging, collision, and growth, they then decrease in volatility (i.e., SF_{mean} increases). This is because these processes can enhance the oxidative level of organics and there are more refractory organics (like polymer-type organics) produced.

For 40 nm particles, the lowest SF_{mean} appeared 2 h later during the Clean2 period (∼ 15:00 LT) than during the Clean1 period (∼ 13:00 LT). This is probably because NPF lasted longer during the Clean2 period. For larger particles, the coating effect of condensable vapors onto pre-existing particles was the major reason behind the intensification of their volatility during NPF events (Wehner et al., 2009; Cheung et al., 2016). The SF_{mean} decreased little compared to that for 40 nm particles. By comparison, the diurnal variation in SF_{mean} for 40 nm particles during the Pollution period changed more smoothly, likely because under a polluted environment the mass fractions of all chemical species were relatively stable (Sun et al., 2016a) and the particles were well-mixed with highly aging levels.

Figure 6b and c show the diurnal variation in SF-PDF for 40 and 150 nm particles. The SF-PDF normally has an NV mode and an SV or VV mode. The NV mode consists of

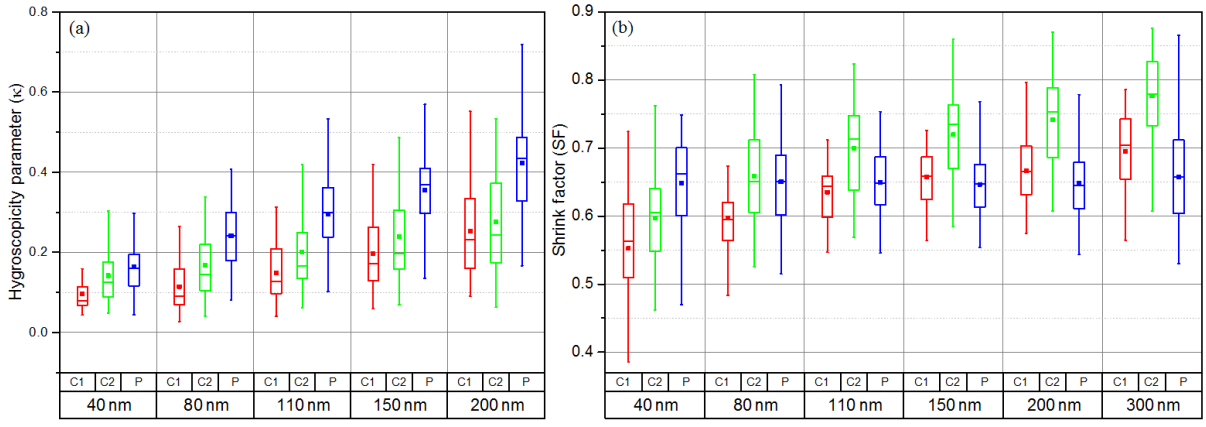

Figure 7. Size-resolved **(a)** κ and **(b)** SF during Clean1 (C1), Clean2 (C2), and Pollution (P) periods. The figure shows the mean κ or SF (solid square markers) with boxes showing the 25th, 50th, and 75th percentiles. The extremities show the 5th and 95th percentiles.

nonvolatile particles, like BC particles, which do not shrink when aerosols are heated. SV and VV modes suggest a mixture of volatile (e.g., organics) and nonvolatile matter that shrink when aerosols are heated (Kuhn et al., 2005). The two SF-PDF modes suggest that the particles during the observed periods were mostly externally mixed. The 40 and 150 nm SF-PDF modes show similar diurnal patterns. During daytime, active aging processes facilitated the mixing of primary particles with secondary species, leading to the transformation of externally mixed particles to internally mixed particles and weakening the NV mode. In particular, this effect was stronger during the Clean1 period than during the other periods. This may be due to the reduction in emissions of soot particles during the control period. In the evening and the early morning, the number fraction of NV-mode particles increased again because a large number of refractory particles (like BC) were emitted from traffic sources or cooking, and then the slower particle aging and weaker vertical mixing made the externally mixed BC accumulate (S. L. Zhang et al., 2016). The number fraction of NV-mode 150 nm particles in the Clean1 case had a stronger increase than that of 40 nm particles in the evening and early morning. This is because freshly emitted refractory particles (like BC) are primarily within the 150 to 240 nm diameter range (Levy et al., 2013). Furthermore, compared with the Pollution case, the number fraction of NV-mode 150 nm particles is much higher during the Clean1 and Clean2 cases. This may reflect the fact that soot particles in a polluted environment can be coated and aged quickly through the heterogeneous reactions of VOCs and other precursor gases (like SO_2, NO_x), which are usually present in extremely high concentrations during polluted days in urban Beijing (Guo et al., 2014; Sun et al., 2016a).

Overall, the diurnal variation in aerosol volatility is different between clean and polluted periods. NPF can enhance volatility through the formation of volatile matter and the coating effect of condensation vapors. Particles observed during the control period showed two significant NV and VV modes during the day, suggesting a more externally mixed state, particularly for the larger particles.

4.3 Size-resolved particle hygroscopic and volatile properties

Table 1 summarizes the size-resolved mean κ, the growth spread factor ($\sigma_{\kappa-\mathrm{PDF}}$) of κ-PDF, size-resolved SF during different periods, and the change in percentages of κ and SF due to the emission control policy. The $\sigma_{\kappa-\mathrm{PDF}}$, defined as the standard deviation of κ-PDF, is an indication of the mixing state of aerosol particles. A higher $\sigma_{\kappa-\mathrm{PDF}}$ generally suggests a higher degree of external mixing (Sjogren et al., 2008; Liu et al., 2011; Jiang et al., 2016). Liu et al. (2011) chose $\sigma_{\kappa-\mathrm{PDF}} = 0.08$ as the cutoff point for high external mixing and quasi-internal mixing. In this study, $\sigma_{\kappa-\mathrm{PDF}}$ always exceeds 0.08 except for the 40 nm particles during the Clean1 period, indicating that the particle population was more externally mixed in urban Beijing. The mean $\sigma_{\kappa-\mathrm{PDF}}$ of 40 nm particles during the Clean1 period is equal to 0.08, suggesting that, during the control period, 40 nm particles had a low degree of external mixing. This is also seen in the quasi-unimodal distribution of 40 nm κ-PDF (Fig. 5b).

During the selected three periods, aerosol particles were more hygroscopic (i.e., κ increased) with increase in particle size (Fig. 7a). The most significant trend is seen in the Pollution case, where κ increases from 0.16 to 0.42 when D_p changes from 40 to 200 nm but only increases from 0.10 to 0.25 for the Clean1 case and from 0.14 to 0.28 for the Clean2 case. This is because particles with a larger size are usually composed of more inorganic salts or oxidized organics, especially in a polluted environment (Swietlicki et al., 2008; Achtert et al., 2009; Fors et al., 2011; Sun et al., 2016a). Meanwhile, the increase in $\sigma_{\kappa-\mathrm{PDF}}$ with the increase in particle size illustrates that there were more external-mixing parti-

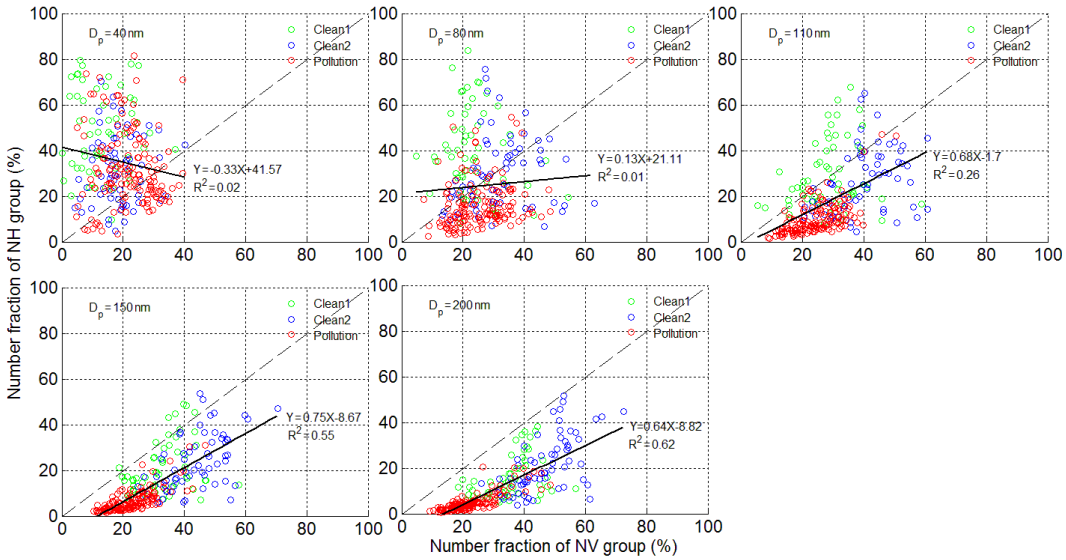

Figure 8. Comparisons between the number fractions of the nearly hydrophobic group (NF_{NH}) and the nonvolatile group (NF_{NV}) for the Clean1 (in green), Clean2 (in blue), and Pollution (in red) periods at the Beijing site (26 August–6 October 2015).

cles with larger sizes (Table 1). Accordingly, aerosol volatility became weaker (SF increased) as particle size increased during the Clean1 and Clean2 periods, but no apparent trend was observed for the Pollution period (Fig. 7b). This finding is consistent with that reported by Wehner et al. (2009).

Figure 6 also shows that all particles were less hygroscopic and more volatile during the control Clean1 period than during the non-control Clean2 period, which can also be seen from the variation in chemical composition. Based on HR-AMS measurements, secondary inorganic aerosols (SIAs) had larger decreases than organic aerosols (OA) during the parade control period. The positive matrix factorization of OA further illustrates that primary OA (POA) had similar decreases as secondary OA (SOA). However, more-oxidized SOA had larger decreases than less-oxidized SOA (Zhao et al., 2017). SIA is always more hydrophilic than OA and more-oxidized SOA is also more hydrophilic than less-oxidized SOA (Jimenez et al., 2009; Chang et al., 2010; Rickards et al., 2013; Zhang et al., 2014; F. Zhang et al., 2016). Therefore, the increased fraction of POA emissions, but weakened age processing due to a sharp reduction in SO_2 and NO_x, leads to particles being less hygroscopic during the control period. Meanwhile, particles become relatively more volatile due to the high number of POA particles because OA volatility is generally inversely correlated with the O : C ratio (an indicator of oxidation state; Jimenez et al., 2009).

To quantify the effects of emission control on aerosol hygroscopicity and volatility, Table 1 also gives the change in percentages of κ and SF during the control Clean1 period compared with that during the non-control Clean2 period. Results show that κ decreased by 32.0–8.5 % from 40 to 200 nm during the control period, with a more significant reduction for small particles, while SF reduced by 7.5–10.5 % from 40 to 300 nm. The significant decrease in aerosol hygroscopicity is favorable for decreasing the aerosol water content, thus suppressing the evolution of regional air pollution (like liquid-phase chemical reaction processes in the atmosphere; Arellanes et al., 2006; Ye et al., 2011; Bian et al., 2014) and eventually improving atmospheric visibility.

4.4 Relationship between nearly hydrophobic and nonvolatile particles

For submicron particles, NV part particles at 300 °C were normally the major NH part particles because both their main components are soot particles (Massling et al., 2009; Wehner et al., 2009). S. L. Zhang et al. (2016) compared the relationship between the number fraction of measured nonvolatile particles (NF_{NV}) and nearly hydrophobic (NF_{NH}) particles and found those two groups are very likely to be dominated by the same component. In this study, we also analyze the relationship of NF_{NH} and NF_{NV} particles as shown Fig. 8.

The results show that Aitken-mode particles (40 and 80 nm) have a very weak linear relationship between NF_{NH} and NF_{NV}, likely because Aitken-mode particles are not as aged. There are a large number of hydrophobic, but volatile, particles such as POA and less-oxidized SOA. Accumulation-mode particles (> 100 nm) show a relatively better linear correlation between NF_{NH} and NF_{NV}, i.e., correlation coefficients (R^2) are 0.26, 0.55, and 0.62 for 110, 150, and 200 nm particles respectively. The higher R^2 for the larger particles may arise because larger particles are highly aged particles from cloud processes. Also, freshly emitted refractory and hydrophobic matter is mostly in the accumulation mode (Levy et al., 2013). The best-fit regression line

for the accumulation-mode particles is always lower than the 1 : 1 line. This can be attributed not only to externally mixed SIA and volatile organics (completely volatile), which are not taken into account for calculation, but also to the fact that some medium-/high-volatile organics are nearly hydrophobic.

There were obvious differences in NF_{NH} and NF_{NV} during the three selected periods. For the Clean1 and Clean2 cases, NF_{NH} and NF_{NV} were larger than those obtained for the Pollution case, but more scatter was seen. This is likely related to the influence of NPF events, during which secondary aerosol material had more complex chemical compositions due to the different sources of precursors. A higher NF_{NH} / NF_{NV} ratio was seen during the Clean1 period than during the other two periods, illustrating a higher number fraction of hydrophobic and volatile particles during the control period.

5 Conclusions and summary

In this study, a H/V-TDMA system was used to measure submicron aerosol hygroscopic and volatile properties in Beijing during and after the parade emission control period. Three periods, namely the control clean period (Clean1), the non-control clean period (Clean2), and the non-control pollution period (Pollution), were selected to study the effect of emission control on aerosol hygroscopicity and volatility.

When emission control measures were in place, particles became more hydrophobic and volatile compared to particles in the non-control period. The κ of 40–200 nm particles decreased by 32.0–8.5 % during the Clean1 period relative to the Clean2 period, while SF of 40–300 nm particles decreased by 7.5–10.5 %. The diurnal variations of κ-PDF were significantly different during the three selected periods, especially for small particles. During the Clean1 period, the κ-PDF of 40 nm particles always showed a quasi-unimodal distribution and had a weaker diurnal variation than that observed during the Clean2 period. This demonstrates that emission control measures can change the diurnal variation pattern of κ-PDF due to the reduction in gas precursors like SO_2 and NO_x, which suppresses the formation of hydrophilic matter. The diurnal variation in aerosol volatility was different between clean and polluted periods. NPF appears to enhance aerosol volatility through the formation of volatile matter and the coating effect of condensable vapors. The particles observed during the control period showed two significant modes during the day, i.e., NV and VV modes, and a more externally mixed state particularly for larger particles.

Aerosol particles became more hygroscopic (i.e., κ increases) as the particle size increased during the three periods. The trend was greatest for the Pollution case where κ increased from 0.16 to 0.42 when D_p changed from 40 nm to 200 nm but only increased from 0.10 to 0.25 for the Clean1 case and from 0.14 to 0.28 for the Clean2 case. Meanwhile, the increase in $\sigma_{\kappa-PDF}$ (i.e., the standard deviation of κ-PDF) with the increase in particle size also illustrates that there were more external-mixing particles with larger sizes. Accordingly, aerosol volatility became weaker (SF increased) as particle size increased during the Clean1 and Clean2 periods, but no apparent trend was observed for the Pollution period.

Our results suggest that emission control measures weaken submicron aerosol hygroscopicity and that aerosol particles are more hygroscopic in a polluted environment. The significant decrease in aerosol hygroscopicity is favorable for suppressing the evolution of regional air pollution. In addition, because of the reduced hygroscopicity, fewer particles would be activated as could condensation nuclei, which is a critical parameter in evaluating the aerosol indirect effect. Thus, our study is important for investigating environmental and climate changes and should inspire both scientists and policy makers to think more deeply about the issue of heavy air pollution in China from a broader perspective.

Data availability. The data in the study are available from the authors upon request (wang.yuying@mail.bnu.edu.cn).

The Supplement related to this article is available online at doi:10.5194/acp-17-5239-2017-supplement.

Competing interests. The authors declare that they have no conflict of interest.

Acknowledgements. This work was funded by the Natural Science Foundation of China (NSFC) research project (grant no. 91544217, 41675141, 41375156), the National Basic Research Program of China "973" (grant no. 2013CB955801), the NSFC-TAMU Collaborative Research Grant Program (grant no. 4141101031), and the National Science Foundation of US (AGS1534670). We also thank all participants in the field campaign for their tireless work and cooperation.

Edited by: R. Zhang
Reviewed by: two anonymous referees

References

Achtert, P., Birmili, W., Nowak, A., Wehner, B., Wiedensohler, A., Takegawa ,N., Kondo, Y., Miyazaki, Y., Hu, M., and Zhu, T.: Hygroscopic growth of tropospheric particle number size distributions over the North China Plain, J. Geophys. Res., 114, D00G07, doi:10.1029/2008jd010921, 2009.

Arellanes, C., Paulson, S. E., Fine, P. M., and Sioutas, C.: Exceeding of Henry's Law by Hydrogen Peroxide Associated with Urban Aerosols, Environ. Sci. Technol., 40, 4859–4866, 2006.

Bian, Y. X., Zhao, C. S., Ma, N., Chen, J., and Xu, W. Y.: A study of aerosol liquid water content based on hygroscopicity measurements at high relative humidity in the North China Plain, Atmos. Chem. Phys., 14, 6417–6426, doi:10.5194/acp-14-6417-2014, 2014.

Chang, R. Y.-W., Slowik, J. G., Shantz, N. C., Vlasenko, A., Liggio, J., Sjostedt, S. J., Leaitch, W. R., and Abbatt, J. P. D.: The hygroscopicity parameter (κ) of ambient organic aerosol at a field site subject to biogenic and anthropogenic influences: relationship to degree of aerosol oxidation, Atmos. Chem. Phys., 10, 5047–5064, doi:10.5194/acp-10-5047-2010, 2010.

Cheung, H. H. Y., Tan, H., Xu, H., Li, F., Wu, C., Yu, J. Z., and Chan, C. K.: Measurements of non-volatile aerosols with a VTDMA and their correlations with carbonaceous aerosols in Guangzhou, China, Atmos. Chem. Phys., 16, 8431–8446, doi:10.5194/acp-16-8431-2016, 2016.

Dall'Osto, M., Harrison, R. M., Coe, H., Williams, P. I., and Allan, J. D.: Real time chemical characterization of local and regional nitrate aerosols, Atmos. Chem. Phys., 9, 3709–3720, doi:10.5194/acp-9-3709-2009, 2009.

Fors, E. O., Swietlicki, E., Svenningsson, B., Kristensson, A., Frank, G. P., and Sporre, M.: Hygroscopic properties of the ambient aerosol in southern Sweden – a two year study, Atmos. Chem. Phys., 11, 8343–8361, doi:10.5194/acp-11-8343-2011, 2011.

Gao, Y., Liu, X., Zhao, C., and Zhang, M.: Emission controls versus meteorological conditions in determining aerosol concentrations in Beijing during the 2008 Olympic Games, Atmos. Chem. Phys., 11, 12437–12451, doi:10.5194/acp-11-12437-2011, 2011.

Guo, S., Hu, M., Zamora, M. L., Peng, J., Shang, D., Zheng, J., Du, Z., Wu, Z., Shao, M., Zeng, L., Molina, M. J., and Zhang, R.: Elucidating severe urban haze formation in China, P. Natl. Acad. Sci. USA, 111, 17373–17378, doi:10.1073/pnas.1419604111, 2014.

Gysel, M., McFiggans, G. B., and Coe, H.: Inversion of tandem differential mobility analyser (TDMA) measurements, J. Aerosol Sci., 40, 134–151, doi:10.1016/j.jaerosci.2008.07.013, 2009.

Hsu, N. C., Gautam, R., Sayer, A. M., Bettenhausen, C., Li, C., Jeong, M. J., Tsay, S.-C., and Holben, B. N.: Global and regional trends of aerosol optical depth over land and ocean using SeaWiFS measurements from 1997 to 2010, Atmos. Chem. Phys., 12, 8037–8053, doi:10.5194/acp-12-8037-2012, 2012.

Huang, K., Zhang, X., and Lin, Y.: The "APEC Blue" phenomenon: Regional emission control effects observed from space, Atmos. Res., 164, 65–75, 2015.

Huang, R., Zhang, Y., Bozzetti, C., Ho, K., Cao, J., Han, Y., Daellenbach, K. R., Slowik, J. G., Platt, S. M., Canonaco, F., Zotter, P., Wolf, R., Pieber, S. M., Bruns, E. A., Crippa, M., Ciarelli, G., Piazzalunga, A., Schwikowski, M., Abbaszade, G., Schnelle-Kreis, J., Zimmermann, R., An, Z., Szidat, S., Baltensperger, U., Haddad, I. E., and Prévôt, A. S. H.: High secondary aerosol contribution to particulate pollution during haze events in China, Nature, 514, 218–222, doi:10.1038/nature13774, 2014.

Jiang, R. X., Tan, H. B., Tang, L. L., Cai, M. F., Yin, Y., Li, F., Liu, L., Xu, H. B., Chan, P. W., Deng, X. J., and Wu, D.: Comparison of aerosol hygroscopicity and mixing state between winter and summer seasons in Pearl River Delta region, China, Atmos. Res., 169, 160–170, 2016.

Jimenez, J. L., Canagaratna, M. R., Donahue, N. M., Prevot, A., Zhang, Q., Kroll, J. H., DeCarlo, P. F., Allan, J. D., Coe, H., and Ng, N. L.: Evolution of organic aerosols in the atmosphere, Science, 326, 1525–1529, 2009.

Kuhn, T., Biswas, S., and Sioutas, C.: Diurnal and seasonal characteristics of particle volatility and chemical composition in the vicinity of a light-duty vehicle freeway, Atmos. Environ., 39, 7154–7166, doi:10.1016/j.atmosenv.2005.08.025, 2005.

Kulmala, M., Vehkamäki, H., Petäjä, T., Dal Maso, M., Lauri, A., Kerminen, V. M., Birmili, W., and McMurry, P. H.: Formation and growth rates of ultrafine atmospheric particles: a review of observations, J. Aerosol Sci., 35, 143–176, doi:10.1016/j.jaerosci.2003.10.003, 2004.

Levy, M. E., Zhang, R., Khalizov, A. F., Zheng, J., Collins, D. R., Glen, C. R., Yuan, W., Yu, X. Y., Winston L., and Jayne, J. T.: Measurements of submicron aerosols in Houston, Texas during the 2009 SHARP field campaign, J. Geophys. Res.-Atmos., 118, 10518–10534, 2013.

Li, H., Zhang, Q., Duan, F., Zheng, B. and, He K.: The "Parade Blue": effects of short-term emission control on aerosol chemistry, Faraday Discuss., 189, 317–335, 2016.

Li, Z., Lau, W. M., Ramanathan, V., Wu, G., Ding, Y., Manoj, M. G., Liu, J., Qian, Y., Li, J., and Zhou, T.: Aerosol and monsoon climate interactions over Asia, Rev. Geophys., 54, 866–929, doi:10.1002/2015RG000500, 2016.

Liu, P. F., Zhao, C. S., Göbel, T., Hallbauer, E., Nowak, A., Ran, L., Xu, W. Y., Deng, Z. Z., Ma, N., Mildenberger, K., Henning, S., Stratmann, F., and Wiedensohler, A.: Hygroscopic properties of aerosol particles at high relative humidity and their diurnal variations in the North China Plain, Atmos. Chem. Phys., 11, 3479–3494, doi:10.5194/acp-11-3479-2011, 2011.

Ma, N., Zhao, C., Tao, J., Wu, Z., Kecorius, S., Wang, Z., Größ, J., Liu, H., Bian, Y., Kuang, Y., Teich, M., Spindler, G., Müller, K., van Pinxteren, D., Herrmann, H., Hu, M., and Wiedensohler, A.: Variation of CCN activity during new particle formation events in the North China Plain, Atmos. Chem. Phys., 16, 8593–8607, doi:10.5194/acp-16-8593-2016, 2016.

Massling, A., Stock, M., Wehner, B., Wu, Z. J., Hu, M., Brüggemann, E., Gnauk, T., Herrmann, H., and Wiedensohler, A.: Size segregated water uptake of the urban submicrometer aerosol in Beijing, Atmos. Environ., 43, 1578–1589, 2009.

Petters, M. D. and Kreidenweis, S. M.: A single parameter representation of hygroscopic growth and cloud condensation nucleus activity, Atmos. Chem. Phys., 7, 1961–1971, doi:10.5194/acp-7-1961-2007, 2007.

Philippin, S., Wiedensohler, A., and Stratmann, F.: Measurements of non-volatile fractions of pollution aerosols with an eight-tube volatility tandem differential mobility analyzer (VTDMA-8), J. Aerosol Sci., 35, 185–203, 2004.

Rickards, A. M. J., Miles, R. E. H., Davies, J. F., Marshall, F. H., and Reid, J. P.: Measurements of the sensitivity of aerosol hygroscopicity and the ê parameter to the O/C ratio, J. Phys. Chem. A, 117, 14120–14131, 2013.

Shi, H., Wang, Y., Chen, J., and Huisingh, D.: Preventing smog crises in China and globally, J. Clean. Prod., 112, 1261–1271, 2016.

Sjogren, S., Gysel, M., Weingartner, E., Alfarra, M. R., Duplissy, J., Cozic, J., Crosier, J., Coe, H., and Baltensperger, U.: Hygroscopicity of the submicrometer aerosol at the high-alpine site Jungfraujoch, 3580 m a.s.l., Switzerland, Atmos. Chem. Phys., 8, 5715–5729, doi:10.5194/acp-8-5715-2008, 2008.

Stolzenburg, M. R. and McMurry, P. H.: TDMAFIT user's manual, University of Minnesota, Department of Mechanical Engineering, Particle Technology Laboratory, Minneapolis, 1–61, 1988.

Stolzenburg, M. R. and McMurry, P. H.: Equations governing single and tandem DMA configurations and a new lognormal approximation to the transfer function, Aerosol Sci. Tech., 42, 421–432, 2008.

Sun, Y., Chen, C., Zhang, Y., Xu, W., Zhou, L., Cheng, X., Zheng, H., Ji, D., Jie, L., and Xiao, T.: Rapid formation and evolution of an extreme haze episode in Northern China during winter 2015, Sci. Rep., 6, 27151, doi:10.1038/srep27151, 2016a.

Sun, Y., Wang, Z., Wild, O., Xu, W., Chen, C., Fu, P., Du, W., Zhou ,L., Zhang, Q., and Han, T.: "APEC Blue": Secondary Aerosol Reductions from Emission Controls in Beijing, Sci. Rep., 6, 20668, doi:10.1038/srep20668, 2016b.

Swietlicki, E., Hansson, H. C., HÄMeri, K., Svenningsson, B., Massling, A., McFiggans, G., McMurry, P. H., PetÄJÄ, T., Tunved, P., Gysel, M., Topping, D., Weingartner, E., Baltensperger, U., Rissler, J., Wiedensohler, A., and Kulmala, M.: Hygroscopic properties of submicrometer atmospheric aerosol particles measured with H-TDMA instruments in various environments—a review, Tellus B, 60, 432–469, doi:10.1111/j.1600-0889.2008.00350.x, 2008.

Tan, H., Xu, H., Wan, Q., Li, F., Deng, X., Chan, P. W., Xia, D., and Yin, Y.: Design and application of an unattended multifunctional H-TDMA system, J. Atmos. Ocean. Tech., 30, 1136–1148, 2013a.

Tan, H., Yin, Y., Gu, X., Li, F., Chan, P. W., Xu, H., Deng, X., and Wan, Q.: An observational study of the hygroscopic properties of aerosols over the Pearl River Delta region, Atmos. Environ., 77, 817–826, 2013b.

Tan, H., Liu, L., Fan, S., Li, F., Yin, Y., Cai, M., and Chan, P. W.: Aerosol optical properties and mixing state of black carbon in the Pearl River Delta, China, Atmos. Environ., 131, 196–208, doi:10.1016/j.atmosenv.2016.02.003, 2016.

Tao, W. K., Chen, J. P., Li, Z., Wang, C., and Zhang, C.: Impact of Aerosols on Convective Clouds and Precipitation, Rev. Geophys., 50, 1–62, 2012.

Wang, T., Nie, W., Gao, J., Xue, L. K., Gao, X. M., Wang, X. F., Qiu, J., Poon, C. N., Meinardi, S., Blake, D., Wang, S. L., Ding, A. J., Chai, F. H., Zhang, Q. Z., and Wang, W. X.: Air quality during the 2008 Beijing Olympics: secondary pollutants and regional impact, Atmos. Chem. Phys., 10, 7603–7615, doi:10.5194/acp-10-7603-2010, 2010.

Wang, Y., Zhang, Q., Jiang, J., Zhou, W., Wang, B., He, K., Duan, F., Zhang, Q., Philip, S., and Xie, Y.: Enhanced sulfate formation during China's severe winter haze episode in January 2013 missing from current models, J. Geophys. Res.-Atmos., 119, 10425–10440, doi:10.1002/2013JD021426, 2014.

Wehner, B., Birmili, W., Ditas, F., Wu, Z., Hu, M., Liu, X., Mao, J., Sugimoto, N., and Wiedensohler, A.: Relationships between submicrometer particulate air pollution and air mass history in Beijing, China, 2004–2006, Atmos. Chem. Phys., 8, 6155–6168, doi:10.5194/acp-8-6155-2008, 2008.

Wehner, B., Berghof, M., Cheng, Y. F., Achtert, P., Birmili, W., Nowak, A., Wiedensohler, A., Garland, R. M., Pöschl, U. and Hu, M.: Mixing state of nonvolatile aerosol particle fractions and comparison with light absorption in the polluted Beijing region, J. Geophys. Res.-Atmos., 114, D00G17, doi:10.1029/2008JD01092, 2009.

Wiedensohler A.: An approximation of the bipolar charge distribution for particles in the submicron size range, J. Aerosol Sci., 19, 387–389, 1988.

Wu, G. X., Li, Z. Q., Fu, C. B., Zhang, X. Y., Zhang, R. Y., Zhang, R. H., Zhou, T. J., Li, J. P., Li, J. D., and Zhou, D. G.: Advances in studying interactions between aerosols and monsoon in China, Science China Earth Science, 59, 1–16, 2016.

Wu, Z. J., Zheng, J., Shang, D. J., Du, Z. F., Wu, Y. S., Zeng, L. M., Wiedensohler, A., and Hu, M.: Particle hygroscopicity and its link to chemical composition in the urban atmosphere of Beijing, China, during summertime, Atmos. Chem. Phys., 16, 1123–1138, doi:10.5194/acp-16-1123-2016, 2016.

Ye, X., Ma, Z., Hu, D., Yang, X., and Chen, J.: Size-resolved hygroscopicity of submicrometer urban aerosols in Shanghai during wintertime, Atmos. Res., 99, 353–364, doi:10.1016/j.atmosres.2010.11.008, 2011.

Zhang, F., Li, Y., Li, Z., Sun, L., Li, R., Zhao, C., Wang, P., Sun, Y., Liu, X., Li, J., Li, P., Ren, G., and Fan, T.: Aerosol hygroscopicity and cloud condensation nuclei activity during the AC^3Exp campaign: implications for cloud condensation nuclei parameterization, Atmos. Chem. Phys., 14, 13423–13437, doi:10.5194/acp-14-13423-2014, 2014.

Zhang, F., Li, Z., Li, Y., Sun, Y., Wang, Z., Li, P., Sun, L., Wang, P., Cribb, M., Zhao, C., Fan, T., Yang, X., and Wang, Q.: Impacts of organic aerosols and its oxidation level on CCN activity from measurement at a suburban site in China, Atmos. Chem. Phys., 16, 5413–5425, doi:10.5194/acp-16-5413-2016, 2016.

Zhang, S. L., Ma, N., Kecorius, S., Wang, P. C., Hu, M., Wang, Z. B., Größ, J., Wu, Z. J., and Wiedensohler, A.: Mixing state of atmospheric particles over the North China Plain, Atmos. Environ., 125, 152–164, doi:10.1016/j.atmosenv.2015.10.053, 2016.

Zhao, J., Du, W., Zhang, Y., Wang, Q., Chen, C., Xu, W., Han, T., Wang, Y., Fu, P., Wang, Z., Li, Z., and Sun, Y.: Insights into aerosol chemistry during the 2015 China Victory Day parade: results from simultaneous measurements at ground level and 260 m in Beijing, Atmos. Chem. Phys., 17, 3215–3232, doi:10.5194/acp-17-3215-2017, 2017.